Further evidence for formation of a narrow baryon resonance with positive strangeness in K^+ collisions with Xe nuclei

DIANA Collaboration

V.V. Barmin[a], A.E. Asratyan[a], V.S. Borisov[a], C. Curceanu[b], G.V. Davidenko[a], A.G. Dolgolenko[a,*], C. Guaraldo[b], M.A. Kubantsev[a,c], I.F. Larin[a], V.A. Matveev[a], V.A. Shebanov[a], N.N. Shishov[a], L.I. Sokolov[a], and G.K. Tumanov[a]

[a] *Institute of Theoretical and Experimental Physics, Moscow 117259, Russia*

[b] *Laboratori Nazionali di Frascati dell' INFN, C.P. 13-I-00044 Frascati, Italy*

[c] *Department of Physics and Astronomy, Northwestern University, Evanston, IL60208, USA*

February 7, 2008

Abstract

We have continued our investigation of the charge-exchange reaction $K^+\mathrm{Xe} \to K^0 p\mathrm{Xe}'$ in the bubble chamber DIANA. In agreement with our previous results based on part of the present statistics, formation of a narrow pK^0 resonance with mass of 1537 ± 2 MeV/c^2 is observed in the elementary transition $K^+n \to K^0p$ on a neutron bound in the Xenon nucleus. Visible width of the peak is consistent with being entirely due to instrumental resolution and allows to place an upper limit on its intrinsic width: $\Gamma < 9$ MeV/c^2. A more precise estimate of the resonance intrinsic width, $\Gamma = 0.36 \pm 0.11$ MeV/c^2, is obtained from the ratio between the numbers of resonant and non-resonant charge-exchange events. The signal is observed in a restricted interval of incident K^+ momentum, that is consistent with smearing of a

*Corresponding author. E-mail address: dolgolenko@itep.ru.

narrow pK^0 resonance by Fermi motion of the target neutron. Statistical significance of the signal is some 7.3, 5.3, and 4.3 standard deviations for the estimators $S/\sqrt{B}$, $S/\sqrt{S+B}$, and $S/\sqrt{S+2B}$, respectively. This observation confirms and reinforces our earlier results, and offers strong evidence for formation of a pentaquark baryon with positive strangeness in the charge-exchange reaction $K^+n \to K^0p$ on a bound neutron.

1 Introduction

The interest in multiquark baryon states was revived by D. Diakonov, V. Petrov, and M. Polyakov [1] who were able to derive fairly definite predictions for the low mass and unusually small width ($\Gamma \leq 15$ MeV/c^2) of the strange pentaquark with $J^P = 1/2^+$ and $S = 1$, the $\Theta^+(1530)$. They were also able to convince the experimentalists of LEPS at SPring-8 and DIANA at ITEP Moscow to test these predictions in low-energy photoproduction and K^+–nucleus collisions, respectively. The enhancements near 1540 MeV/c^2 in the nK^+ and pK^0 effective-mass spectra, that were almost simultaneously detected by LEPS [2] and DIANA [3], touched off a wave of experimental searches for the Θ^+ baryon that yielded positive observations as well as null results (the rapidly evolving experimental situation is described in, *e.g.,* [4]). Recently, the CLAS experiment reported null results of high-statistics searches for the Θ^+ in photoproduction on hydrogen [5] and deuterium [6]. In the BELLE experiment at the KEKB asymmetric e^+e^- collider, interactions of secondary particles with detector material were used for studying the charge-exchange reaction $K^+n \to K^0p$ in the K^+ momentum region below some 2 GeV/c. No signal from formation of the Θ^+ baryon was observed, and an upper limit on the Θ^+ intrinsic width was imposed: $\Gamma < 0.64$ MeV/c^2 for $m(\Theta^+) = 1539$ MeV/c^2 [7]. On the other hand, the LEPS and SVD-2 experiments were able to confirm their earlier positive observations at higher statistical levels in γD collisions with $E_\gamma \leq 2.4$ GeV [8] and in pA collisions at $E_p = 70$ GeV [9], respectively.

The charge-exchange reaction $K^+n \to K^0p$ on a bound neutron, that is investigated by DIANA [3] and BELLE [7], is particularly interesting because it allows to probe the Θ^+ intrinsic width in a model-independent manner [10, 12, 11, 13]. Yet another important advantage of the latter process is that the strangeness of the final-state pK^0_S system is *a priori* known to be positive. In this paper, we update the results reported in [3] by analyzing a bigger sample of the charge-exchange reaction $K^+n \to K^0p$ in low-energy

K^+Xe collisions.

2 The experiment and the data

The bubble chamber DIANA filled with liquid Xenon was exposed to a separated K^+ beam with momentum of 850 MeV/c from the 10-GeV ITEP proton synchrotron. The density and radiation length of the fill are 2.2 g/cm^3 and 3.7 cm, respectively. The chamber has a total volume of $70 \times 70 \times 140$ cm^3 viewed by photographic cameras, and operates without magnetic field [14]. Charged particles are identified by ionization and momentum-analyzed by range in Xenon. In the fiducial volume of the bubble chamber, K^+ momentum is a function of longitudinal coordinate and varies from 750 MeV/c for entering kaons to zero for those that range out through ionization. (A 150-mm-thick layer of Xenon downstream of the front wall is excluded from the fiducial volume, and is only used for detecting the secondaries that travel in the backward hemisphere.) Throughout this interval of K^+ momentum, partial cross sections for formation of various final states of K^+Xe collisions can be measured thanks to efficient detection of both the decays and interactions of incident kaons in the Xenon bubble chamber. The momentum of an interacting K^+ is determined from longitudinal position of the interaction vertex with respect to central position of the observed maximum due to decays of stopping K^+ mesons. The uncertainty on K^+ momentum, $p_{\rm beam}$, decreases with increasing $p_{\rm beam}$ and is near 20 MeV/c for the momentum interval of 450–550 MeV/c. The estimate of K^+ momentum based on measured position of the interaction vertex has been verified by detecting and reconstructing the $K^+ \to \pi^+\pi^+\pi^-$ decays in flight, which provided an independent estimate of K^+ momentum.

On total, some 10^6 tracks of incident K^+ mesons are recorded on film. Scanning of the film yielded nearly 35 000 events with visible K^0 decays, $K^0_S \to \pi^+\pi^-$ and $K^0_S \to \pi^0\pi^0$, that could be associated with primary K^+Xe vertices with different multiplicities of secondary particles. For each event with a K^0 candidate, longitudinal coordinate of the primary vertex was measured at the scanning stage. Finally, events with a single proton and $K^0_S \to \pi^+\pi^-$ in the final state were selected as candidates for the charge-exchange reaction $K^+n \to K^0p$ without rescatterings. In order to reduce the total volume of measurements, a lower cutoff was imposed on the K^+ track length before interaction (see further). The selected events are then fully measured and reconstructed in space using specially designed stereo-projectors similar to those proposed in [15]. In particular, we

measure the K^0_S and proton emission angles with respect to the K^+ direction, π^+ and π^- emission angles with respect to the parent K^0_S direction, and proton and pion paths in Xenon.

The momentum is estimated by range for the proton, and by pion ranges and emission angles for the K^0_S. In order to reduce the uncertainties on measured momenta and emission angles, protons with $p_p < 180$ MeV/c and K^0_S mesons with $p_K < 170$ MeV/c are dropped, and the distance between the primary vertex and the K^0_S decay vertex is required to exceed 2.5 mm. On average, experimental resolution is near 2% for the K^0 and proton momenta, and $\sim 2^0$ for the angle between their directions in the lab system. Further details on the experimental procedure can be found in [16, 17]. The quality of the data is best reflected by experimental resolution on effective mass of the pK^0 system, estimated as $\sigma_m \simeq 3.0$ MeV/c^2 from the simulation. The latter estimate is consistent with the width of the $\Lambda \to p\pi^-$ peak measured in a previous experiment with the same detector [18, 3].

This work is based on a sample of 2131 fully measured events of the charge-exchange reaction $K^+\mathrm{Xe} \to K^0 p\mathrm{Xe}'$, that comprises the "old" data analyzed in [3] as well as the "new" data analyzed here for the first time. The K^+ range before interaction was required to exceed 550 mm for the "old" data, and 520 mm for the "new" data. On average, this corresponds to K^+ momentum cutoffs of $p_{\mathrm{beam}} < 530$ and 560 MeV/c, respectively (the correspondence is not exact since beam momentum varied by some ± 20 MeV/c in different exposures). For all measured events of the reaction $K^+\mathrm{Xe} \to K^0 p\mathrm{Xe}'$, momentum spectra of incident kaons are separately plotted for the old and new data in Fig. 1. Note that compared to our earlier analysis [3], the statistics of the charge-exchange reaction has nearly doubled, and mean K^+ momentum has increased from 470 to 500 MeV/c. Expanding the range of K^+ momentum allows to probe the lineshape of the putative pK^0 resonance that is smeared by Fermi motion of the target nucleon, see further.

3 The simulation and the effects of rescattering

Rescattering of either the K^0 or proton in the Xenon nucleus distorts the effective mass of the pK^0 system originally formed in the charge-exchange reaction $K^+n \to K^0p$. In order to suppress the background arising from rescatterings, the following selections were used in our previous analysis [3]: $\Theta_p < 100^0$, $\Theta_K < 100^0$, and $\Phi > 90^0$. Here, Θ_K and Θ_p are

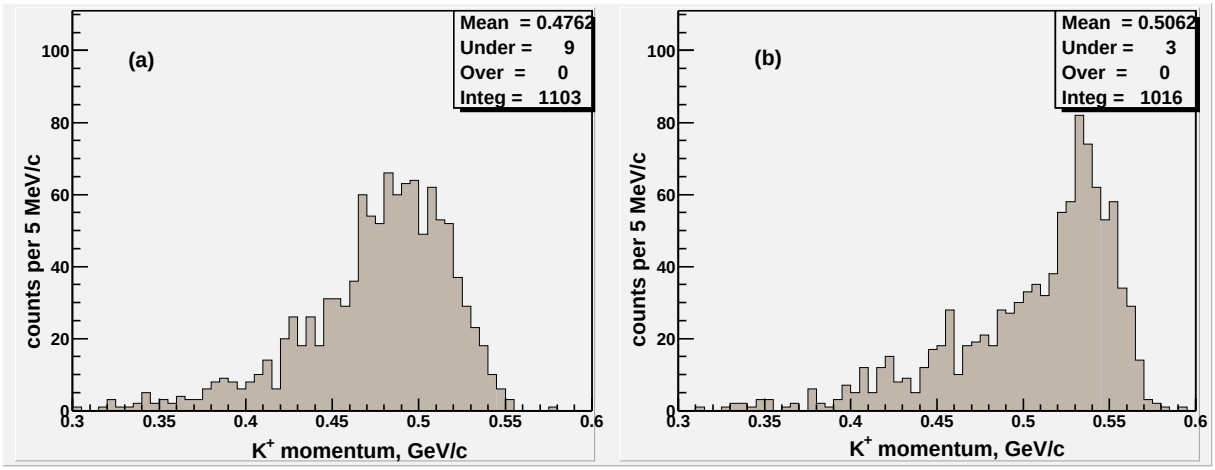

Figure 1: Incident K^+ momentum for measured events of the reaction $K^+\mathrm{Xe} \to K^0 p\mathrm{Xe}'$. The old and new data are shown in (a) and (b), respectively.

the K^0 and proton emission angles with respect to the K^+ direction in the lab system, and Φ is the angle between the K^0 and proton in the plane normal to beam direction. The validity of these selections was verified by the theoretical analysis [19].

We demonstrate the rejection power of the above selections to rescatterings using a simple Monte-Carlo simulation of the charge-exchange reaction $K^+n \to K^0p$ in nuclear environment. In the simulation, total energy of a bound neutron is parametrized as $E_n = m_N - 2\epsilon - p_n^2/(2m_N)$, where m_N is the mass of a free neutron, ϵ is the mean binding energy, and p_n is Fermi momentum [19]. For the Xenon nucleus, we assume $\epsilon = 7$ MeV and use a realistic form of the Fermi-momentum distribution with maximum near 170 MeV/c. The flux of incident K^+ mesons as a function of K^+ momentum is inferred from the observed distribution of K^+ range in Xenon before interaction or decay, see [3]. The effects of apparatus resolution and measurement errors are included in the simulation. Rescattering in the nucleus is not accounted for. In the distributions to follow, the number of simulated events is normalized to that of observed ones prior to cuts.

We find that the selections $\Theta_p < 100^0$, $\Theta_K < 100^0$, and $\Phi > 90^0$ reject some 12% of the simulated rescattering-free events ($\sim 11\%$ without $\Phi > 90^0$), and as much as $\sim 46\%$ of all live events of the reaction $K^+n \to K^0p$ detected in our experiment. This shows that the above selections significantly reduce the fraction of rescattered events in the sample. For the binary reaction considered, it is straightforward to estimate the mass of the effective target, $m_{\mathrm{targ}}^{\mathrm{eff}}$. The $m_{\mathrm{targ}}^{\mathrm{eff}}$ distributions of live and simulated events prior to cuts, for the selections $\Theta_p < 100^0$ and $\Theta_K < 100^0$ only, and for the full selections $\Theta_K, \Theta_p < 100^0$

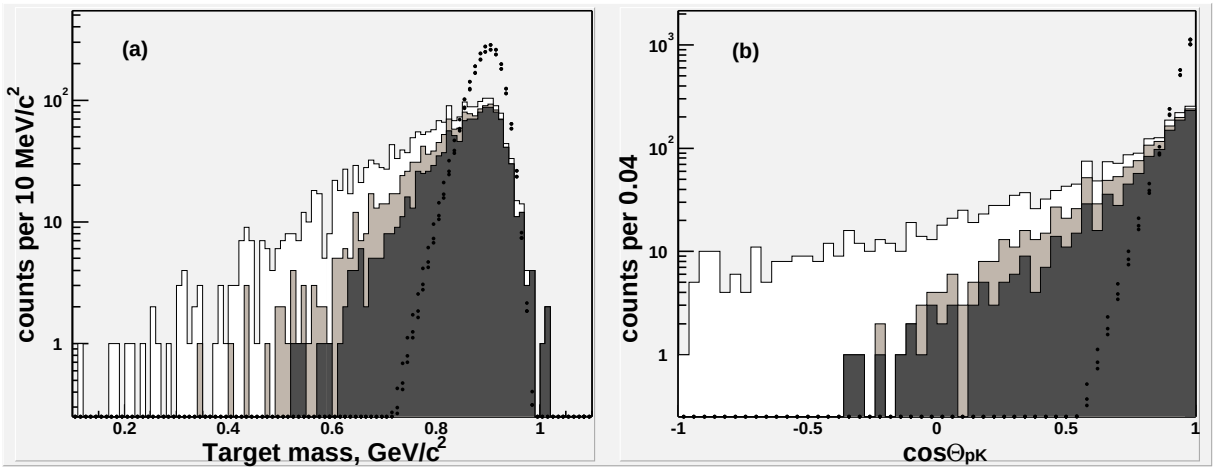

Figure 2: The mass of effective target (a) and the angle between the pK^0 and K^+ directions in the lab system (b) for observed and simulated events (simulated distributions are depicted by dots). The middle histograms (light-shaded and dotted) are for the selections $\Theta_p < 100^0$ and $\Theta_K < 100^0$ only. The bottom histograms (dark-shaded and dotted) are for the full selections $\Theta_K, \Theta_p < 100^0$ and $\Phi > 90^0$.

and $\Phi > 90^0$ are shown in Fig. 2a. The observed $m^{\rm eff}_{\rm targ}$ distribution reaches a maximum near that of the simulated distribution, but shows a long downward tail that is due to rescatterings, see Fig. 2a. The aforementioned selections are seen to substantially reduce the width of the $m^{\rm eff}_{\rm targ}$ distribution by rejecting rescatterings. Cosine of the angle between the pK^0 and incident K^+ directions in the lab frame, Θ_{pK}, is plotted in Fig. 2b. Due to rescatterings, live pK^0 systems are typically emitted at broader angles to the K^+ beam than the simulated ones. Again, the aforementioned angular selections lead to a better agreement between the observed and simulated distributions. It is interesting to see how the rescatterings affect the angular distribution in the pK^0 center-of-mass frame. Cosine of the K^0–K^+ angle in the pK^0 rest frame, $\Theta^{\rm cm}_K$, is shown in Fig. 3a. Prior to selections, the $\cos\Theta^{\rm cm}_K$ distribution of live events monotonically decreases between -1 and +1, whereas that of simulated events is almost forward–backward symmetric (the dips towards the boundary values are due to lower cuts on the K^0 and proton momenta, see above). The selections $\Theta_p < 100^0$, $\Theta_K < 100^0$, and $\Phi > 90^0$ are seen to restore the agreement between the simulated and observed $\cos\Theta^{\rm cm}_K$ distributions by suppressing rescatterings. Alternatively, the (approximate) forward–backward symmetry of the $\cos\Theta^{\rm cm}_K$ distribution is restored by applying other selections suggested by the simulation: $\cos\Theta_{pK} > 0.6$ or $m^{\rm eff}_{\rm targ} > 750$ MeV/c^2 (see Figs. 3b and 3c).

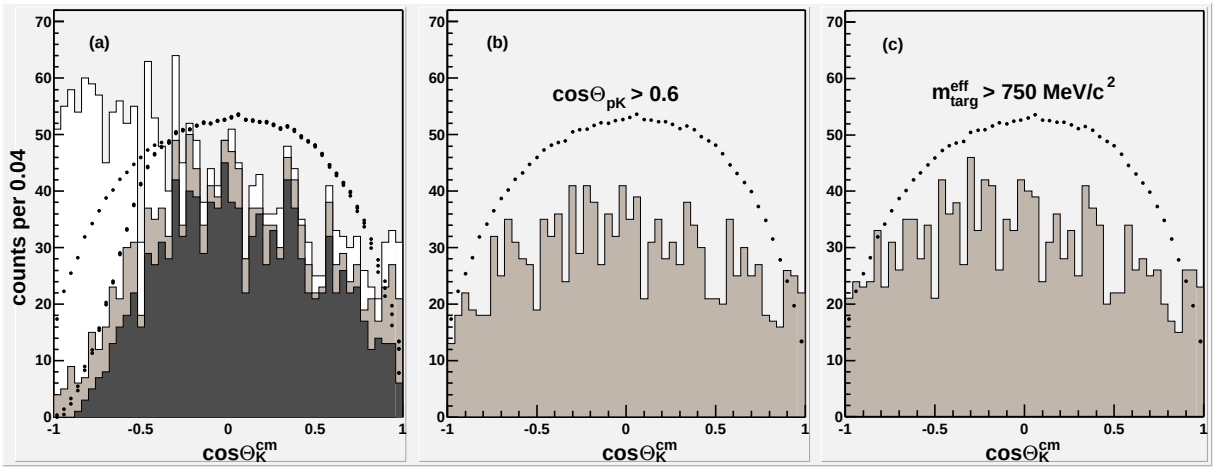

Figure 3: Cosine of the K^0–K^+ angle in the pK^0 rest frame, $\Theta_K^{\rm cm}$, for observed and simulated events (simulated distributions are depicted by dots). In (a), the middle histograms (light-shaded and dotted) are for the selections $\Theta_p < 100^0$ and $\Theta_K < 100^0$ only, and the bottom histograms (dark-shaded and dotted) are for the full selections $\Theta_K, \Theta_p < 100^0$ and $\Phi > 90^0$. The alternative selections $\cos\Theta_{pK} > 0.6$ and $m_{\rm targ}^{\rm eff} > 750$ MeV/c^2 result in the observed and simulated $\cos\Theta_K^{\rm cm}$ distributions shown in (b) and (c), respectively.

4 The pK^0 effective-mass distributions

The initial stage of this analysis is to approximate the experimental conditions of [3], and to use exactly the same selections as in [3], in order to see what happens with the putative signal. So here we apply the selection $p_{\rm beam} < 530$ MeV/c that corresponds to the effective $p_{\rm beam}$ cutoff for the old data. Effective mass of the K^0p system formed in the charge-exchange reaction, $m(pK_S^0)$, is shown in Fig. 4a. (Note that because of the cut $p_{\rm beam} < 530$ MeV/c, relative contribution of the "new" data is only $\simeq 37\%$ in Fig. 4a.) Prior to selections aimed at suppressing the background from proton and K^0 rescattering in the Xenon nucleus, but a small enhancement is seen in the mass region of 1535–1540 MeV/c^2. The selections $\Theta_p < 100^0$, $\Theta_K < 100^0$, and $\Phi > 90^0$ reduce the pK^0 effective-mass spectrum to the shaded histogram shown in the same Figure. These selections are seen to emphasize the enhancement in the mass region of 1535–1540 MeV/c^2. The latter $m(pK_S^0)$ distribution is then fitted to a Gaussian on top of a fifth-order polynomial, see Fig. 4b. The width of the observed peak is compatible with experimental resolution on $m(pK_S^0)$. Compared to [3] where a signal of ~ 30 events above background at $m(pK_S^0)$ $= 1539\pm2$ MeV/c^2 was reported, we now observe a substantially bigger signal at a slightly smaller pK^0 effective mass. Analogous $m(pK_S^0)$ distributions for the full interval of $p_{\rm beam}$ are shown in Figs. 4c and 4d. Adding events with $p_{\rm beam} > 530$ MeV/c results in a broader

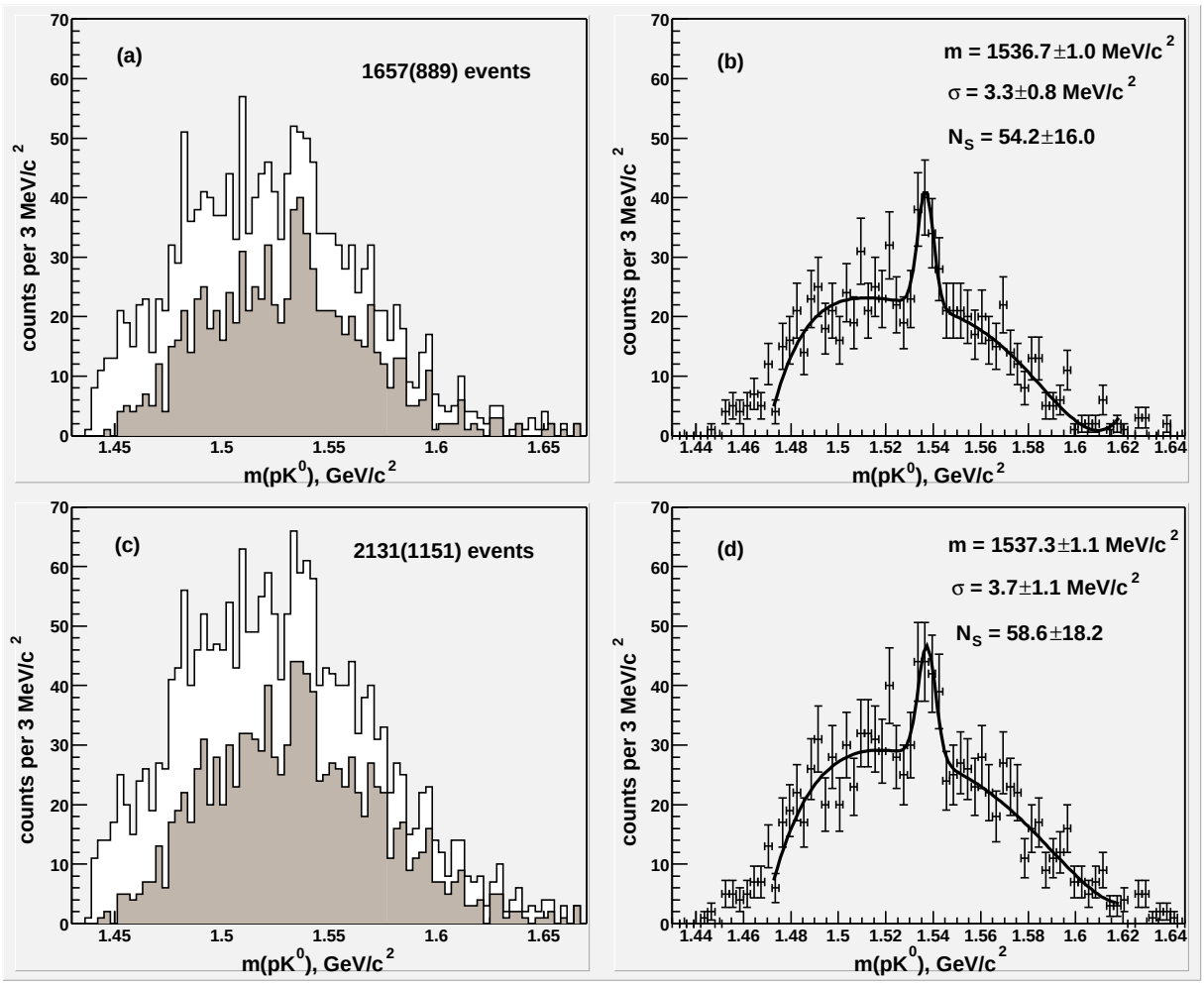

Figure 4: Effective mass of the pK^0 system formed in the reaction $K^+\mathrm{Xe} \to K^0 p\mathrm{Xe}'$ for $p_{\mathrm{beam}} < 530$ MeV (a) and for the full range of p_{beam} (c). Shaded histograms result from the selections $\Theta_p < 100^0$, $\Theta_K < 100^0$, and $\Phi > 90^0$. In (b) and (d), corresponding shaded histograms are fitted to a Gaussian on top of a fifth-order polynomial.

enhancement and a higher level of background.

It is interesting to study the dependence of the putative signal on incident K^+ momentum, p_{beam}. Note that a narrow pK^0 resonance would produce a line in the p_{beam} distribution for $K^+n \to K^0p$ if the target neutron were free rather than bound, whereas the Fermi motion would smear the above line to a lineshape of finite width. On the Monte-Carlo level, we simulate formation of a narrow pK^0 resonance with mass of 1537 MeV/c^2 by selecting events in the $m(pK^0_S)$ interval of 1537$\pm$2 MeV/c^2 as the resonant contribution to the charge-exchange reaction $K^+n \to K^0p$. The simulated ratio between the resonant and non-resonant contributions to $K^+n \to K^0p$ as a function of K^+ momentum, that is independent of the K^+ flux, is shown in Fig. 5 (arbitrary units). Despite the smearing,

the peak is seen to survive in the form of a broad asymmetric maximum near the resonant value of $p_{\rm beam}$ for a free target neutron. Now, multiplying the $p_{\rm beam}$ distribution of all detected charge-exchange events by the aforementioned ratio, we are able to estimate the $p_{\rm beam}$ distribution for a narrow pK^0 resonance with $m = 1537$ MeV/c^2 in our experimental conditions, see Fig. 5. The lineshape of the assumed resonance has a smaller width than the $p_{\rm beam}$ distribution of all $K^+n \to K^0p$ events, which suggests that a true resonant signal should benefit from restricting the range of K^+ momentum.

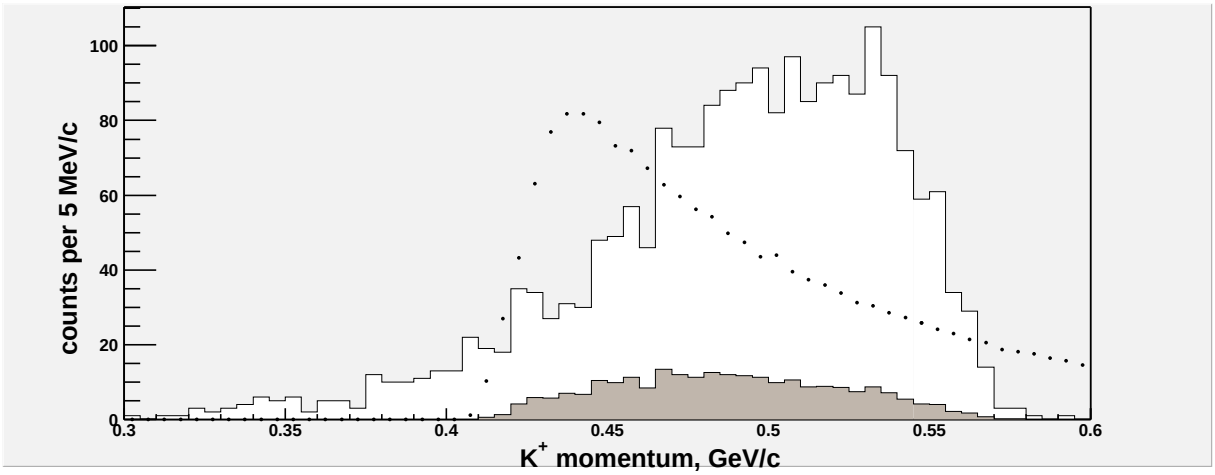

Figure 5: Open histogram: incident K^+ momentum for all measured events of the charge-exchange reaction $K^+n \to K^0p$. Dotted histogram: for an assumed narrow pK^0 resonance with mass of 1537 MeV/c^2, the simulated ratio between the resonant and non-resonant contributions to $K^+n \to K^0p$ as a function of K^+ momentum (in arbitrary units). Shaded histogram: predicted lineshape of the assumed pK^0 resonance. For definiteness, the latter distribution has been normalized to the number of live events in the mass interval $1532 < m(pK^0) < 1544$ MeV/c^2 prior to selections.

Restricting the K^+ momentum to the interval $445 < p_{\rm beam} < 525$ MeV/c, that is consistent with Fermi-smearing of a narrow resonance, results in a prominent peak near 1537 MeV/c^2 in the pK^0 effective-mass spectrum, see Fig. 6a. Fitted width of the peak is again consistent with being entirely due to apparatus smearing of the pK^0 effective mass. The $m(pK^0_S)$ distributions for the momentum intervals $p_{\rm beam} < 445$ MeV/c and $p_{\rm beam} > 525$ MeV/c are structureless, see Figs. 6c and 6d. The latter is in contradiction with the claim [20] that the pK^0 peak reported in [3] is a kinematic artifact of K^+n collisions on quasifree neutrons. Similar $m(pK^0_S)$ distributions but for the selections $\Theta_p < 100^0$ and $\Theta_K < 100^0$ only, that is, with the cut $\Phi > 90^0$ lifted, are shown in Fig. 7. Lifting the selection $\Phi > 90^0$ leaves the peak near 1537 MeV/c^2 virtually unaffected, but broadens the background under the peak. Statistical significance of the signal in Fig. 7b is near 7.3,

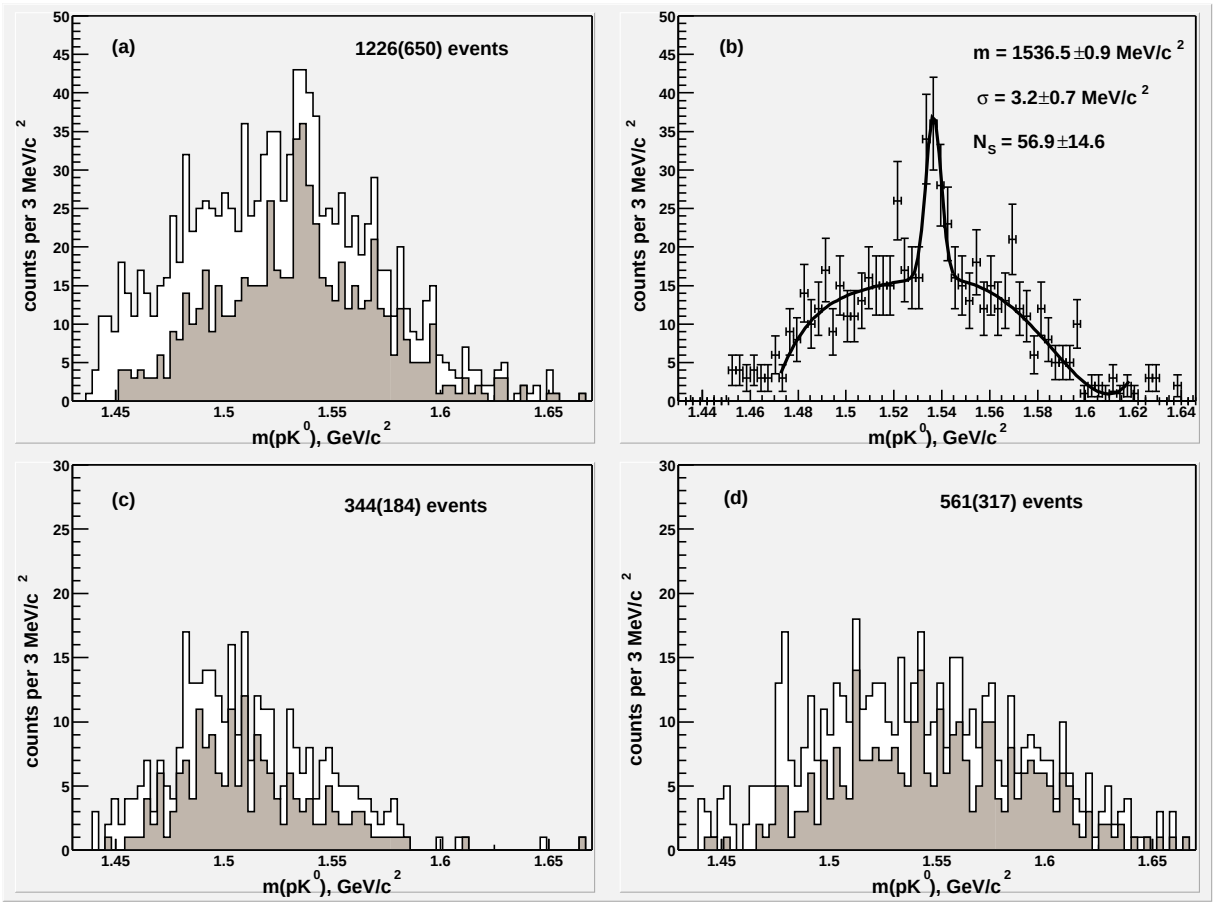

Figure 6: Effective mass of the K^0p system for $445 < p_{\rm beam} < 525$ MeV/c (a), $p_{\rm beam} < 445$ MeV/c (c), and $p_{\rm beam} > 525$ MeV/c (d). Shaded histograms are for the selections $\Theta_p < 100^0$, $\Theta_K < 100^0$, and $\Phi > 90^0$. Shown in (b) is a fit of the shaded distribution in (a) to a Gaussian on top of a fifth-order polynomial.

5.3, and 4.3 standard deviations for the estimators $S/\sqrt{B}$, $S/\sqrt{S+B}$, and $S/\sqrt{S+2B}$, respectively. Here, $B \simeq 68$ events and $S \simeq 60$ events are the fitted background and the excess above background in the mass interval $1532 < m(pK^0) < 1544$ MeV/c^2 that is consistent with the instrumental resolution on $m(pK^0_S)$.

The data of Figs. 3 and 2 suggest the feasibility of alternative selections. The $m(pK^0_S)$ distributions for $445 < p_{\rm beam} < 525$ MeV/c, plotted under either $\cos\Theta_{pK} > 0.6$ or $m^{\rm eff}_{\rm targ} > 750$ MeV/c^2, are shown in Figs. 8a and 8b, respectively. Under either selection, the distribution of the center-of-mass angle $\Theta^{\rm cm}_K$ is flatter for the live than simulated events, see Fig. 3. The latter suggests that the background fraction increases towards the edges, $\cos\Theta^{\rm cm}_K = \pm 1$. Therefore, we use an additional selection $|\cos\Theta^{\rm cm}_K| < 0.6$ in

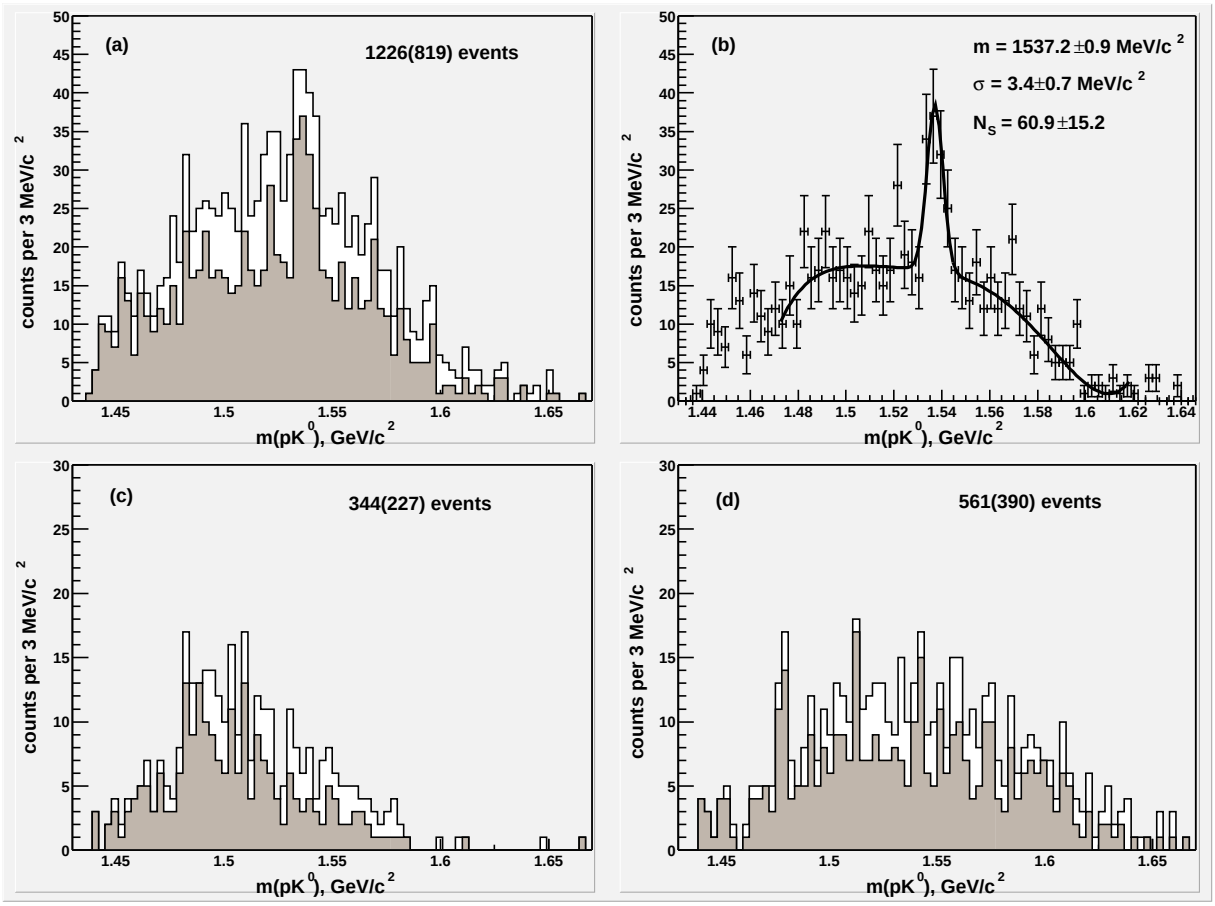

Figure 7: Similar $m(pK^0_S)$ distributions as in Fig. 6, but shaded histograms are for the selections $\Theta_p < 100^0$ and $\Theta_K < 100^0$ only (that is, the selection $\Phi > 90^0$ is lifted).

conjunction with either $\cos\Theta_{pK} > 0.6$ or $m^{\rm eff}_{\rm targ} > 750$ MeV/c^2. Either combined selection rejects $\sim 30\%$ of simulated $K^+n \to K^0p$ events. The resulting pK^0 mass spectra for $445 < p_{\rm beam} < 525$ MeV/c, that are illustrated and fitted in Fig. 8, show prominent peaks similar to that in Fig. 6b. The corresponding $m(pK^0_S)$ distributions for the K^+ momentum intervals $p_{\rm beam} < 445$ MeV/c and $p_{\rm beam} > 525$ MeV/c (not shown) again prove to be featureless. We find that absolute momentum of the effective target, $p^{\rm eff}_{\rm targ}$, is strongly correlated with $m^{\rm eff}_{\rm targ}$, so that the selection $m^{\rm eff}_{\rm targ} > 750$ MeV/c^2 is roughly equivalent to $p^{\rm eff}_{\rm targ} < 400$ MeV/c (corresponding $m(pK^0_S)$ distributions are not shown here).

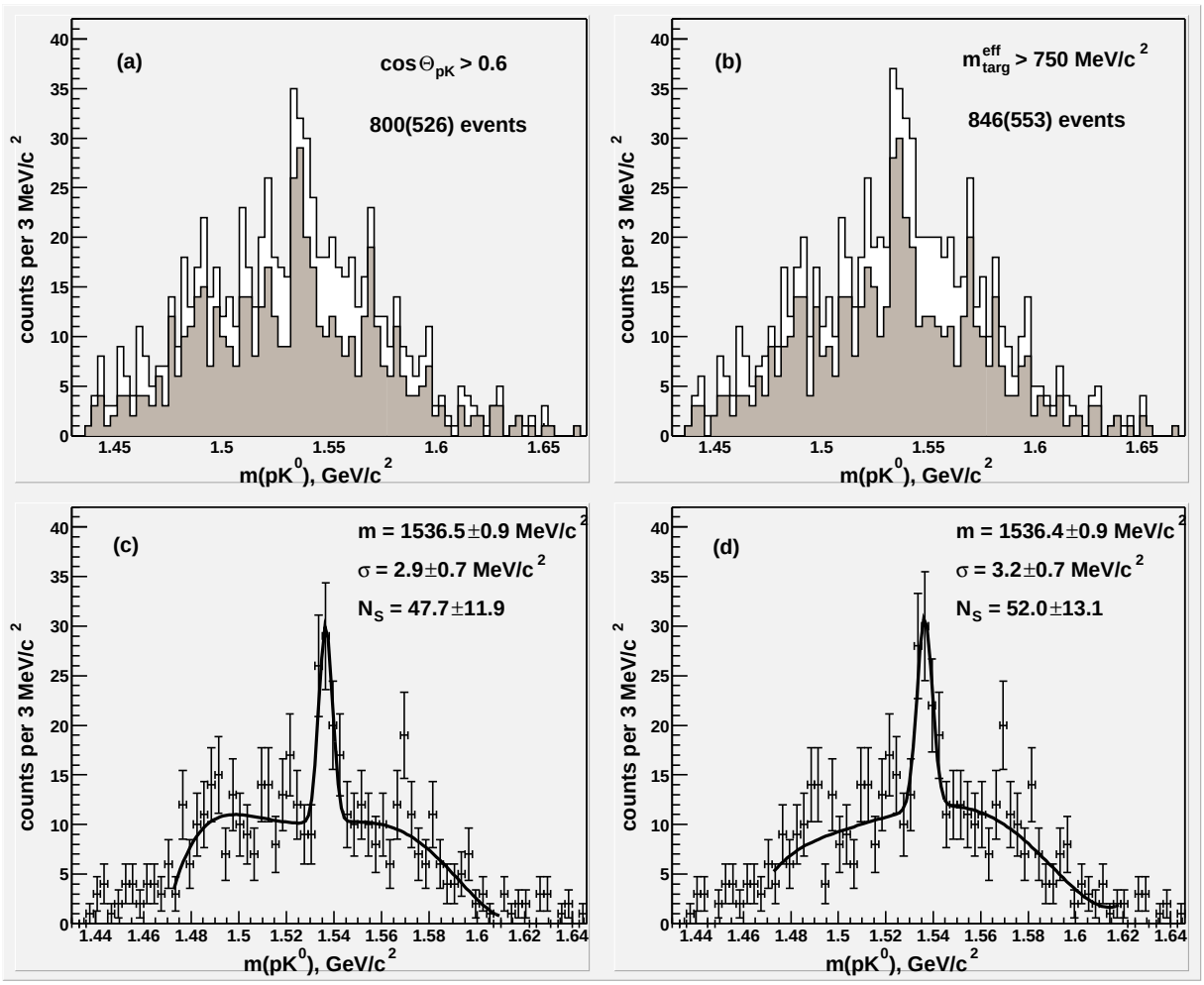

Figure 8: Effective mass of the K^0p system for $445 < p_{\rm beam} < 525$ MeV/c, plotted under the selections $\cos\Theta_{pK} > 0.6$ (a) or $m^{\rm eff}_{\rm targ} > 750$ MeV/c^2 (b). Shaded histograms are for the additional selection $|\cos\Theta^{\rm cm}_K| < 0.6$. Fits of the latter distributions are shown in (c) and (d).

5 Intrinsic width of the Θ^+ baryon

The width of the observed pK^0 peak is consistent with being entirely due to instrumental smearing and allows to place an upper limit on intrinsic width: $\Gamma < 9$ MeV/c^2. On the other hand, intrinsic width of a pK^0 resonance formed in the charge-exchange reaction $K^+n \to K^0p$ can be determined as [11]

$$\Gamma = \frac{N^{\rm peak}}{N^{\rm bkgd}} \times \frac{\sigma^{\rm CE}}{107{\rm mb}} \times \frac{\Delta m}{B_i B_f},$$

where $N^{\rm peak}$ and $N^{\rm bkgd}$ are numbers of events in the peak and in the charge-exchange background under the peak, $\sigma^{\rm CE} = 4.1 \pm 0.3$ mb is the cross section for $K^+n \to K^0p$

[21], B_i and B_f are branching fractions for the initial and final states ($B_i = B_f = 1/2$), and Δm is the $m(pK^0_S)$ interval under the peak that is populated by $N^{\rm bkgd}$ background events. From the signal-to-background ratio observed in our previous analysis [3], the Θ^+ width was estimated in [11] as $\Gamma = 0.9 \pm 0.3$ MeV/c^2. The assumption was made that the cuts adopted in [3] reduced the resonant and non-resonant charge-exchange processes by the same factor, and systematic uncertainties associated with rescattering in the nucleus could not be evaluated. But as soon as the Θ^+ decay width is ~ 1 MeV or less, the bulk of produced Θ^+ baryons will decay outside of the nucleus giving rise to pK^0 pairs that are not affected by rescatterings. The latter assumption is indirectly supported by the data: we see that expanding the $p_{\rm beam}$ interval beyond the resonant region rapidly degrades the signal-to-background ratio while the Θ^+ signal remains the same within errors. So for a self-consistent determination of Γ, the "original" rather than observed number of nonresonant pK^0 pairs under the Θ^+ peak should be substituted in the above formula.

We estimate the non-resonant pK^0 background not distorted by rescatterings from the simulated $m(pK^0_S)$ distribution, applying the selections $\Theta_K, \Theta_p < 100^0$ and $445 < p_{\rm beam} < 525$ MeV/c as in Fig. 7. In the K^+ momentum unterval $445 < p_{\rm beam} < 525$ MeV/c, the number of simulated events prior to experimental selections and angular cuts is normalized to the original number of all charge-exchange collisions with $K^0_S \to \pi^+\pi^-$ in the final state. The latter is estimated as 4060 ± 400 collisions from the scanning information. Of these events, $(60 \pm 7)\%$ are estimated to survive upon rejecting K^0_S mesons with $L < 2.5$ mm, protons and K^0_S mesons that have reinteracted in liquid Xenon, and unmeasurable events. Normalizing the number of simulated events to 2440 ± 370 live events, we then apply the cuts $p_K > 170$ MeV/c, $p_p > 180$ MeV/c, $\Theta_p < 100^0$, and $\Theta_K < 100^0$ on the Monte-Carlo level assuming no rescattering in the nucleus. Thereby, the "original" non-resonant background in the mass region $1532 < m(pK^0) < 1544$ MeV/c^2 is estimated as $N^{\rm bkgd} \simeq 310 \pm 47$ events. Substituting this value in the above formula together with the observed signal for the same selections, $N^{\rm peak} = 60 \pm 15$ events, we obtain $\Gamma = 0.36 \pm 0.11$ MeV/c^2 where the error does not include systematic uncertainties of the simulation procedure. This experimental estimate has been obtained assuming that the bulk of produced Θ^+ baryons neither decay nor reinteract inside the nucleus. Our estimate of the Θ^+ intrinsic width does not contradict the upper limit set by BELLE [7].

6 Summary and conclusions

To summarize, a narrow pK^0 resonance has been observed in the charge-exchange reaction $K^+n \to K^0p$ on a neutron bound in the Xenon nucleus. The mass of the resonance is estimated as $m = 1537 \pm 2$ MeV/c^2. Visible width of the peak, $\sigma = 3.4 \pm 0.7$ MeV/c^2, is consistent with being entirely due to instrumental resolution and allows to place an upper limit on intrinsic width: $\Gamma < 9$ MeV/c^2. A more precise estimate of the resonance intrinsic width, $\Gamma = 0.36 \pm 0.11$ MeV/c^2, has been obtained from the ratio between the numbers of resonant and non-resonant charge-exchange events. The signal is observed in a restricted interval of incident K^+ momentum, that is consistent with smearing of a narrow pK^0 resonance by Fermi motion of the target neutron. With an excess of ~ 60 events over a fitted background of ~ 68 events, statistical significance of the signal is some 7.3, 5.3, and 4.3 standard deviations for the estimators $S/\sqrt{B}$, $S/\sqrt{S+B}$, and $S/\sqrt{S+2B}$, respectively. We interpret this observation as strong evidence for formation of a pentaquark baryon with positive strangeness in the charge-exchange reaction $K^+n \to K^0p$ on a bound neutron. The results reported in this paper confirm and reinforce our earlier observation based on part of the present statistics of the charge-exchange reaction [3]. The measurements and data analysis are still in progress.

We wish to thank K. Boreskov, A. Kudryavtsev, T. Nakano, I. Strakovsky, G.H. Trilling, and M. Zhalov for stimulating discussions and useful comments. This work is supported by the Russian Foundation for Basic Research (grant 04-02-17467).

References

[1] D. Diakonov, V. Petrov, and M. Polyakov, Z. Phys. A359, 305 (1997).

[2] T. Nakano et al. (LEPS Coll.), Phys. Rev. Lett. 91, 012002 (2003), hep-ex/0301020.

[3] V.V. Barmin et al. (DIANA Coll.), Yad. Fiz. 66, 1763 (2003), Phys. Atom. Nucl. 66, 1715 (2003), hep-ex/0304040.

[4] Volker D. Burkert, hep-ph/05010309.

[5] M. Battaglieri et al. (CLAS Coll.), Phys. Rev. Lett. 96, 042001 (2006), hep-ex/0510061.

[6] B. McKinnon et al. (CLAS Coll.), hep-ex/0603028.

[7] R. Mizuk et al. (BELLE Coll.), Phys. Lett. B632, 173 (2006).

[8] T. Hotta (for the LEPS Coll.), Acta Phys. Polon. B36, 2173 (2005); T. Nakano, talk presented at the Int. Conf. on QCD and Hadronic Physics, Beijing, China, June 2005.

[9] A. Aleev et al. (SVD-2 Coll.), NPI MSU 2005-22/788, hep-ex/0509033.

[10] R.A. Arndt, I.I. Strakovsky, and R.L. Workman, Phys. Rev. C68, 042201 (2003).

[11] R.N. Cahn and G.H. Trilling, Phys.Rev. D69, 011501 (2004).

[12] W. Gibbs, Phys. Rev. C70, 045208 (2004).

[13] A. Sibirtsev et al., Phys. Lett. B599, 230 (2004), hep-ph/0405099.

[14] V.V. Barmin et al., Prib. Tekhn. Eksp. 4, 61 (1984).

[15] J.W. Cronin et al., Phys. Rev. Lett. 18, 25 (1967).

[16] V.V. Barmin et al., Nucl. Phys. A556, 409 (1993).

[17] V.V. Barmin et al., Phys. At. Nucl. 57, 1655 (1994).

[18] V.V. Barmin et al., Nucl. Phys. A683, 305 (2001).

[19] A. Sibirtsev et al., Eur. Phys. J. A23, 491 (2005).

[20] M. Zavertyaev, hep-ph/0311250.

[21] U. Casadei et al., CERN–HERA 75-1.